Predicting Wind Turbine Blade Loads using Vorticity Transport and RANS Methodologies

Timothy M. Fletcher* Richard E. Brown† DaHye Kim‡ Oh Joon Kwon§

Rotor Aeromechanics Laboratory
Department of Aerospace Engineering
University of Glasgow, Glasgow, G12 8QQ, UK
Tel: +44 141 330 6479, Fax: +44 141 330 5560

Computational Aerodynamics Laboratory
Department of Aerospace Engineering
KAIST, Daejeon 305-701, Korea
Tel: +82 42 869 3720, Fax: +82 42 869 3710

Two computational methods, one based on the solution of the vorticity transport equation, and a second based on the solution of the Reynolds-Averaged Navier-Stokes equations, have been used to simulate the aerodynamic performance of a horizontal axis wind turbine. Comparisons have been made against data obtained during Phase VI of the NREL Unsteady Aerodynamics Experimental and against existing numerical data for a range of wind conditions. The Reynolds-Averaged Navier-Stokes method demonstrates the potential to predict accurately the flow around the blades and the distribution of aerodynamic loads developed on them. The Vorticity Transport Model possesses a considerable advantage in those situtations where the accurate, but computationally efficient, modelling of the structure of the wake and the associated induced velocity is critical, but where the prediction of blade loads can be achieved with sufficient accuracy using a lifting-line model augmented by incorporating a semi-empirical stall delay model. The largest benefits can be extracted when the two methods are used to complement each other in order to understand better the physical mechanisms governing the aerodynamic performance of wind turbines.

Nomenclature

c	aerofoil chord
C_n	normal force coefficient, $= F_n / \frac{1}{2}\rho c(V_\infty^2 + (\Omega r)^2)$
C_p	pressure coefficient
C_t	tangential force coefficient, $= F_t / \frac{1}{2}\rho c(V_\infty^2 + (\Omega r)^2)$
F_n	sectional normal force
F_t	sectional tangential force (+ve forward)
P_∞	freestream static pressure
P_0	local stagnation pressure
Q	shaft torque
R	rotor radius
r	radial distance
V_∞	wind speed
z	axial distance
λ	tip speed ratio, $= \Omega R / V_\infty$
ρ	density
Ω	rotor rotational speed

*Post-doctoral Research Asst., t.fletcher@eng.gla.ac.uk
†Mechan Chair of Engineering, rbrown@eng.gla.ac.uk
‡Graduate Research Asst., ssseer@kaist.ac.kr
§Professor, ojkwon@kaist.ac.kr

Presented at the European Wind Energy Conference & Exhibition, Parc Chanot, Marseille, France, 16–19 March 2009.

Introduction

Aerodynamicists rely on a spectrum of computational tools when analysing the performance of wind turbines, ranging from blade-element – momentum theory and free-wake codes, to Navier-Stokes solvers. The wide range of tools that are commonly used for the aerodynamic simulation of wind turbines remain in use because each offers its own advantages, whether it be predicting the complex fluid dynamics on the blades to a high fidelity, or providing 'ball-park' performance estimates with a minimal overhead in terms of computational cost. This paper will introduce two computational schemes that are now being applied to the simulation of wind turbine aerodynamics, one based on the solution of the vorticity transport equation, and a second based on the solution of the Reynolds-Averaged Navier-Stokes equations.

The aerodynamic loading on the blades, the velocity and pressure distributions over the blades, and the wake structure that is predicted by each of the two computational schemes will be compared against each other, and against data from Phase VI of the NREL Unsteady Aerodynamics Experiment [1]. A significant number of re-

searchers have published numerical predictions of the Phase VI test cases in the past, including, for example, the full Navier-Stokes simulations performed by Sezer-Uzol [2], and Sørensen, Michelsen and Schreck [3]. In addition, a number of works have enabled considerable progress to be made in understanding better the details of the flow around wind turbine blades. The aim of this paper is not to perform a validation exercise *per se*, but rather to show how two quite different approaches to the simulation of wind turbine aerodynamics can be used to complement each other and to yield insight which exceeds that which is possible from the application of each method in isolation.

Vorticity Transport Model

The Vorticity Transport Model (VTM) developed by Brown [4], and extended by Brown and Line [5], enables the simulation of wind turbine aerodynamics and performance using a high-fidelity model of the wake that is generated by the turbine rotor. After making the physically realistic assumption of incompressibility within the wake, the Navier-Stokes equations are cast into the vorticity-velocity form

$$\frac{\partial}{\partial t}\omega + u \cdot \nabla\omega - \omega \cdot \nabla u = S + \nu\nabla^2\omega \qquad (1)$$

and are then discretised in finite-volume form using a structured Cartesian mesh within the domain surrounding the turbine. The advection, stretching and diffusion terms within the vorticity transport equation describe the changes in the vorticity field, ω, with time at any point in space, as a function of the velocity field, u, and the viscosity, ν. The physical condition that vorticity may neither be created nor destroyed within the flow, and thus may only be created at the solid surfaces immersed within the fluid, is accounted for using the vorticity source term, S. The vorticity source term is determined as the sum of the temporal and spatial variations in the bound vorticity, ω_b, on the turbine blades, given a flow velocity relative to the blade, u_b:

$$S = -\frac{d}{dt}\omega_b + u_b \nabla \cdot \omega_b \qquad (2)$$

The bound vorticity distribution on the blades of the rotor is modelled using an extension of lifting-line theory. The velocity field is related to the vorticity field by using a Cartesian fast multipole method to invert the differential form of the Biot-Savart law:

$$\nabla^2 u = -\nabla \times \omega \, . \qquad (3)$$

Use of the fast multipole method, in conjunction with an adaptive grid in which cells are only present within the calculation when the vorticity within them is non-zero, dramatically increases the computational efficiency of the scheme when compared to an equivalent calculation performed on a fixed grid. In the current analysis, the ground plane is not modelled and therefore the velocity gradient associated with the atmospheric boundary layer does not influence the flow field surrounding the turbine. The method is rendered effectively boundary-free as cells may be created, when necessary, on a Cartesian stencil which extends to infinity, using the assumption that there is zero vorticity outside the wake. An assumption is made that the Reynolds number within the computational domain is sufficiently high that the governing flow equation may be solved in inviscid form (so that ν=0). Dissipation of the wake does still occur, however, through the mechanism of natural vortical instability. The numerical diffusion of vorticity within the flow field surrounding the turbine is kept at a very low level by using a Riemann problem technique based on the Weighted Average Flux method developed by Toro (see Ref. 4) to advance Eq. 1 through time. This approach allows the structure of the wake to be captured at significantly larger wake ages, without significant spatial smearing of the wake structure, than is possible when using more conventional computational fluid dynamics (CFD) techniques based on the pressure-velocity-density formulation of the Navier-Stokes equations.

Reynolds-Averaged Navier-Stokes Method

Complementary simulations have been performed using a three-dimensional, incompressible, Reynolds-Averaged Navier-Stokes (RANS) flow solver developed at the Korean Advanced Institute for Science and Technology (KAIST) by Kwon *et al.* [6,7]. By using an artificial compressibility method [8], the Navier-Stokes equations may be written in an integral form for an arbitrary solution domain V, with boundary ∂V, as

$$\frac{\partial}{\partial \tau}\int_V \vec{Q} dV + \widetilde{K}\frac{\partial}{\partial t}\int_V \vec{Q} dV + \oint_{\partial V} \vec{F}(Q) \cdot \vec{n} dS = \oint_{\partial V} \vec{G}(Q) \cdot \vec{n} dS \, , \qquad (4)$$

where $\vec{Q}$ is the vector of primitive variables, and $\vec{F}(Q)\cdot\vec{n}$ and $\vec{G}(Q)\cdot\vec{n}$ are the inviscid and viscous flux vectors normal to ∂V, respectively. Time t is the physical time used for time-accurate calculations, whilst τ is the pseudo-time used to advance steady simulations to convergence. $\widetilde{K}$ is the identity matrix. The governing equations are discretised using a vertex-centred finite-volume method in which each control volume is composed of the median duals surrounding the corresponding vertex. The inviscid flux terms are computed using the flux-difference splitting scheme developed by Roe (see Ref. 7), whilst the viscous flux terms are computed by adopting a modified central difference method. Implicit time integration is performed using a linearised Euler backward difference scheme of second order. The linear system of equations is solved at each time step using a point Gauss-Seidel method. The Spalart-Allmaras one-equation turbulence model is used to estimate the eddy viscosity, and the flow is assumed to be fully turbulent in all of the RANS simulations presented in this paper.

The no-slip boundary condition was imposed on the surface of the blade, whilst at the far-field boundary a characteristic boundary condition was applied. The turbulent viscosity for the Spalart-Allmaras model was extrapolated from the interior on outflow boundaries and was specified to be equal to the freestream value on inflow boundaries. The freestream eddy viscosity was taken to be 10% of the laminar viscosity.

Table 1: NREL Phase VI Rotor Data

Type of rotor	rigid
No. of blades	2
Rotor radius	5.029m
Aerofoil	NREL S809
Rotational speed	72rpm (constant)
Blade tip pitch	3°

Wind Turbine Models

The two-bladed rotor tested during Phase VI of the NREL Unsteady Aerodynamics Experiment was simulated in the present study [1]. A detailed description of the blade geometry and test conditions is given by Hand *et al.* [1]; but the key properties of the turbine rotor are summarised in Table 1. The structural deformation of the blades, in the form of bending, torsion and extension, are not modelled in the current analysis, and the blades are rigidly attached to the hub. In addition, the aerodynamic effects associated with the hub assembly and tower have not been modelled.

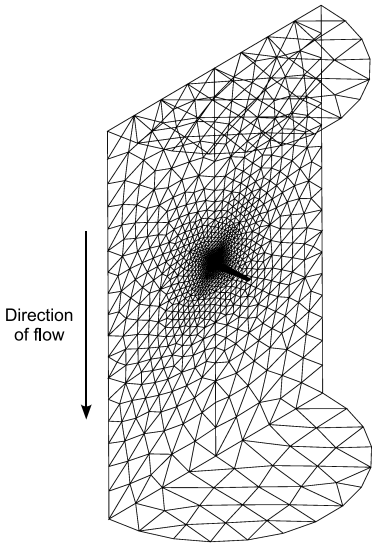

Figure 1: *Surface triangulation at the boundaries of the computational mesh on which the Navier-Stokes calculations were performed.*

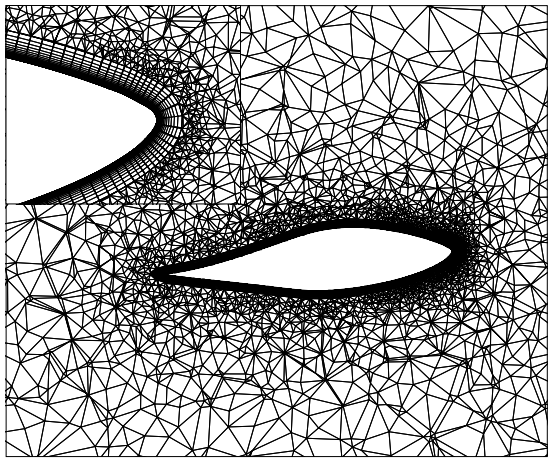

Figure 2: *Cross-section (at the 0.8R radial location) through the computational mesh on which the Navier-Stokes calculations were performed. Inset: detail of the hybrid computational mesh near to the leading edge of the blade.*

Steady RANS simulations were performed of a single turbine blade operating in axial wind conditions. A periodic boundary condition was applied to represent the influence of the first blade on the second. The Reynolds-Averaged Navier-Stokes calculations were performed using far-field

boundaries located three rotor radii both upstream and downstream of the rotor, and, in the radial direction, at a distance of three rotor radii from the axis of rotation. Figure 1 shows the full computational domain and demonstrates the periodicity of the grid that is created by the surface triangulation at the grid boundaries. Figure 2 shows a sectional view, at a radial location of 0.8R, through the hybrid mesh used for the RANS simulations. To capture accurately the flow inside the boundary layer, a layer of prismatic elements, with a depth of thirty prisms, is created surrounding the blade surface, structured such that there is an increase in prism height with distance from the blade surface of 25% in each successive prism. The remainder of the computational domain was populated using tetrahedral elements.

Blade Aerodynamic Loading

When a horizontal axis wind turbine operates at a high tip speed ratio, the local flow velocity over the blades is predominantly parallel to the chord and remains largely attached to the surface of the blade along most of the span. In contrast, at low tip speed ratios, separation occurs on the suction surface of the blade and the flow aft of the separation line is largely in the radial direction, toward the tip of the blade. Indeed, the considerable variabilities in the flow experienced by wind turbine blades across their operational envelope poses considerable challenges to the simulation of their aerodynamics.

Simulation codes that use a lifting-line or lifting-surface model to compute the effective distribution of angle of attack along the blades, and hence the aerodynamic loading, are highly sensitive to the two-dimensional 'static' aerofoil data that is necessarily provided as an input to the simulation. Past comparisons have revealed distinct variability in the distributions of lift and drag coefficient as a function of angle of attack measured during seemingly very similar wind tunnel tests [9]. The variation in the maximum lift coefficient, the (static) post stall lift coefficient, and the lift curve slope when comparing data sets measured in different wind tunnel tests has been shown to be larger even than the variations associated with Reynolds number. Duque, Burkland and Johnson [10] demonstrated, by making specific comparisons with the NREL Phase VI experimental data, that a stall delay model must be applied to the two-dimensional aerofoil data in lifting-line codes in order to obtain accurate predictions of the aerodynamic loading on the blades at low

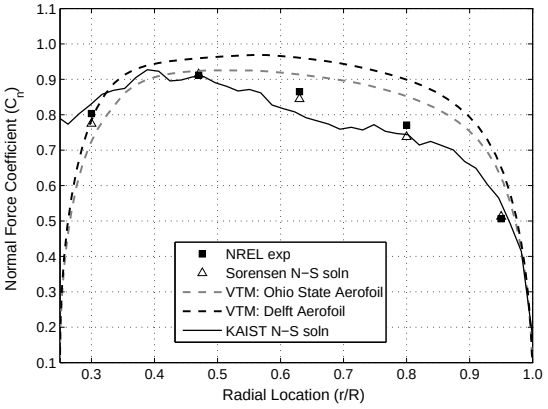

(a) Wind speed 7m/s (λ=5.4)

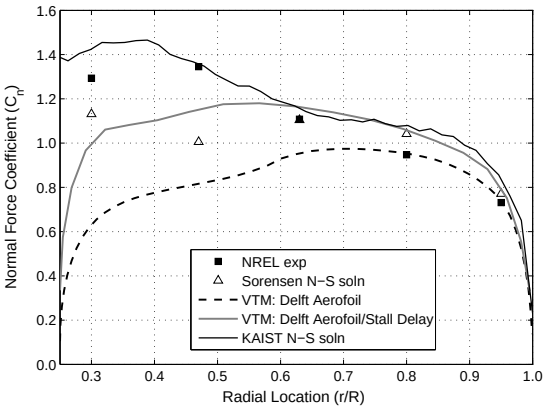

(b) Wind speed 10m/s (λ=3.8)

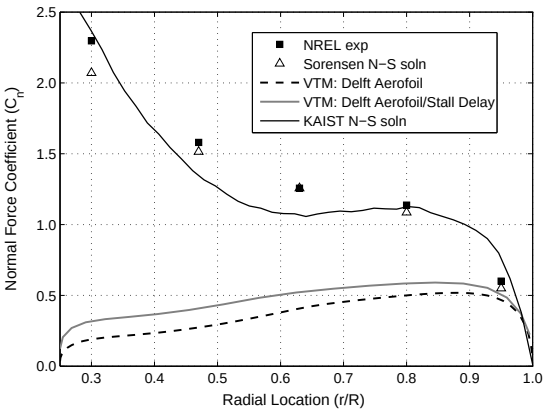

(c) Wind speed 25m/s (λ=1.5)

Figure 3: *Radial distribution of normal force coefficient.*

tip speed ratios (at wind speeds greater than approximately 7m/s for the Phase VI rotor). A comprehensive comparison of stall delay models was provided by Breton, Coton and Moe [11], in which it was noted that although several of the stall delay models that have been developed offer large improvements in the accuracy of load predictions at intermediate wind speeds, there is no single

stall delay model that enables comprehensive improvements over the full range of wind speeds. When solving the Navier-Stokes equations to resolve fully the velocity and pressure fields surrounding the wind turbine blades, the solution does not rely on empirical inputs. Care must be taken though to ensure the use of a computational grid of sufficient quality and an appropriate choice of turbulence model in order to achieve good comparions with experimental results.

Figures 3 and 4 show the variation of normal and tangential force coefficient along the length of the NREL blade, respectively, when the rotor is operating in axial winds of speed 7, 10, and 25m/s. For each of the three wind conditions shown in Figs. 3 and 4, force coefficient data is shown from the NREL Phase VI experiment, the Reynolds-Averaged Navier-Stokes simulations performed previously by Sørensen [3], the current Reynolds-Averaged Navier-Stokes simulations, and the Vorticity Transport Model. The VTM was used in conjunction with two-dimensional aerodynamic performance data for the S809 aerofoil that was measured during wind tunnel tests performed by Delft University of Technology [12].

The Sørensen and KAIST RANS solutions demonstrate excellent agreement with the experimental data at a wind speed of 7m/s, as shown in Figs. 3(a) and 4(a). Good agreement is shown between the data obtained during the VTM computations and the experimental data, with only a modest over-prediction of normal and tangential force coefficients along the outboard half of the blade. Distributions of normal and tangential force coefficient computed using the VTM with two alternative sets of wind tunnel data for the S809 aerofoil are shown in Figs. 3(a) and 4(a) for comparison. The use of the Delft, rather than the Ohio State, aerofoil data results in a modest increase in the over-prediction of aerodynamic loads by the VTM, and demonstrates the sensitivity to prescribed aerofoil characteristics that was alluded to earlier. The distribution of the angle of attack along the blades in a 7m/s wind predicted by the VTM indicates that almost all sections along the length of the blade operate within the linear, pre-stall aerodynamic regime. A stall delay model, therefore, has no effect on the predictions of the aerodynamic loading on the blades.

Figures 3(b) and 4(b) show a comparison of the computed radial distributions of normal and tangential force coefficient with those measured during the NREL experiments at a wind speed of 10m/s. In addition, together with the predictions obtained using uncorrected aerofoil data,

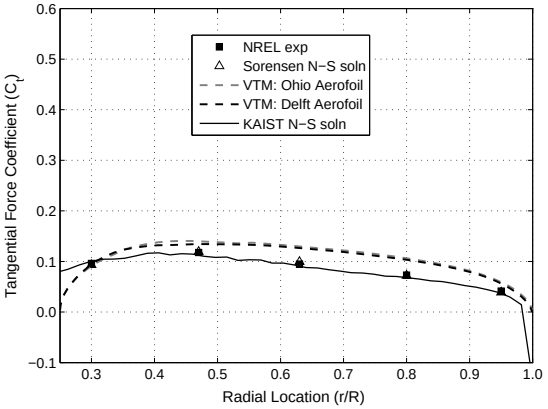

(a) Wind speed 7m/s (λ=5.4)

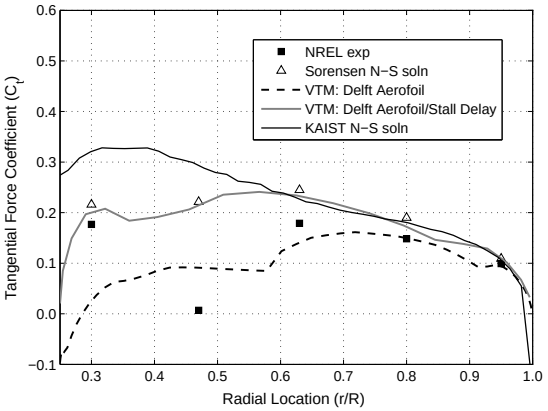

(b) Wind speed 10m/s (λ=3.8)

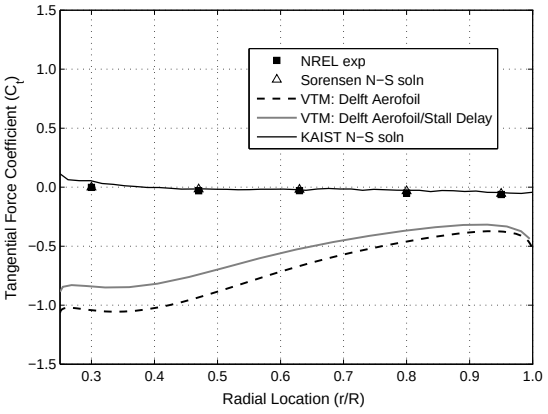

(c) Wind speed 25m/s (λ=1.5)

Figure 4: *Radial distribution of tangential force coefficient.*

Figs. 3(b) and 4(b) also show the normal and tangential force calculated using the VTM following the application of the Corrigan and Schillings [13] stall delay model. When the VTM is used without the stall delay model, there is significant under-prediction of the normal force coefficient on the inboard portion of the blade, despite excellent agreement with the experimental data at the 0.8R

and 0.95R radial stations, as shown in Fig. 3(b). A significant improvement in the correlation of normal force coefficient with the NREL experimental data is obtained along the inboard portion of the blade when the VTM is used in conjunction with the Corrigan and Schillings stall delay model. Unfortunately, a corresponding over-prediction arises along the outboard portion of the blade. The distribution of normal force coefficient predicted using the KAIST RANS code represents a small over-prediction in normal force coefficient along both the inboard part of the blade and towards the tip of the blade. It is clear from Fig. 3(b) that accurate predictions of normal force coefficient along the outboard portion of the blade are often accompanied by poor predictions further inboard. This observation also applies to the prediction of tangential force coefficient, as demonstrated by Fig. 4(b). Furthermore, despite the obvious advantages to applying a stall delay model to modify two-dimensional aerofoil data for the effects of three-dimensional flow, Figs. 3(b) and 4(b) also demonstrate the potential perils of 'chasing' the experimental data when choosing a stall delay model, and specifically when identifying the coefficients that are to be used when applying semi-empirical models such as these.

The substantial under-prediction, by the VTM, of the normal force coefficient along the blade operating in a 25m/s wind, shown in Fig. 3(c), demonstrates the limitations of the Corrigan and Schillings stall delay model. In addition, when the turbine rotor operates in a 25m/s wind, large negative values of tangential force coefficient are computed by the VTM, along the majority of the blade, even with the use of the stall delay model, as shown in Fig. 4(c). This distribution of force was not observed in the experiment and, in practice, would act to retard the blades, significantly reducing the torque developed by the rotor.

The distributions of normal and tangential force coefficient on the blades when operating in a 25m/s wind that were computed using the KAIST RANS code compare well with the predictions made by Sørensen, as shown in Figs. 3(c) and 4(c). In particular, the reduced tangential force on the blades that is demonstrated in Fig. 4(c) compared to that evident at lower wind speeds indicates a significant flow separation over a large portion of the suction surface of the blade. The predicted extent of this separation is entirely consistent with the NREL experimental data, and may suggest that the KAIST and Sørensen RANS codes provide higher fidelity predictions when simulating a fully-separated rather than a partially-separated flow over the blades.

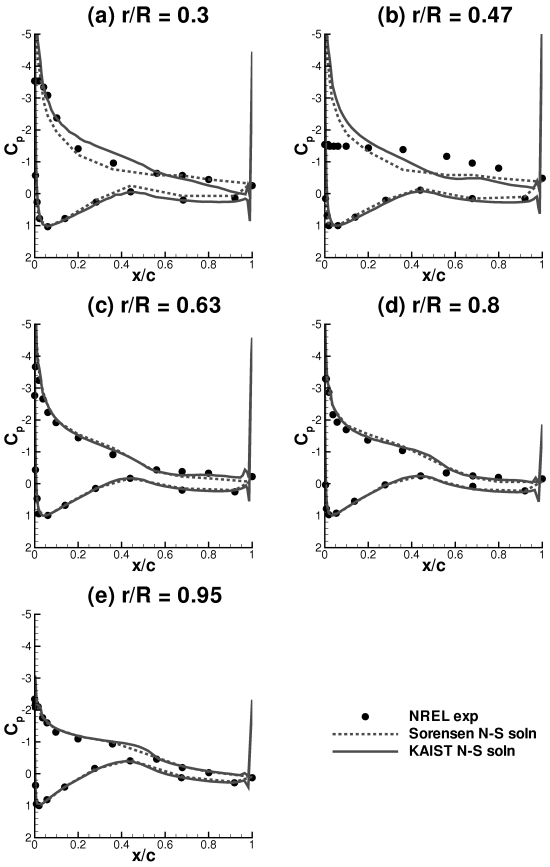

Figure 5: *Chordwise distribution of pressure coefficient when operating in a 10m/s wind (λ=3.8).*

In the current RANS calculations, the Spalart-Allmaras turbulence model was used without a model for the laminar-to-turbulent transition near the leading edge of the blade. When the wind turbine operates within a 10m/s wind, however, transition may play a critical role in dictating the chordwise location at which the flow separates. It is reasonable to consider, therefore, that the discrepancy between the aerodynamic loading on the blades computed using the KAIST RANS code and the experimental data may be attributed to the fact that no transition model was used, and the subsequent mis-representation of the growth of the boundary layer near the leading edge.

Surface Pressure and Velocity

The variations in the normal and tangential components of the force on the blades with wind speed and radial location can be understood better by an examination of the distributions of pressure and flow velocity on the blade surface. Numerical schemes such as the VTM, that utilise a

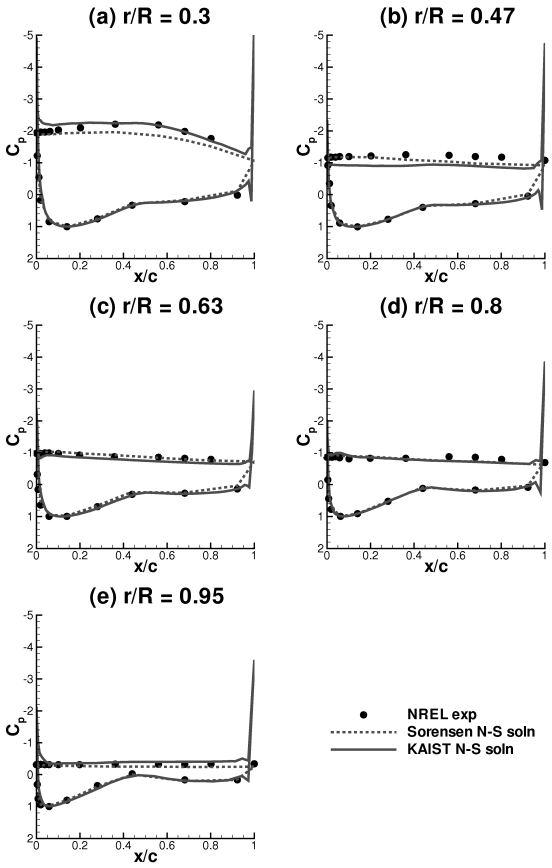

Figure 6: *Chordwise distribution of pressure coefficient when operating in a 25m/s wind (λ=1.5).*

lifting-line model for the blade aerodynamics, naturally allow the extraction of the angle of attack distribution along the quarter-chord line. Only limited information can be extracted, however, regarding the fluid dynamics near the surface of the blades, and usually only by inference from the two-dimensional performance data for the aerofoil. In RANS simulations, however, the distribution of pressure and velocity over the entire blade surface is computed directly.

Figures 5 and 6 show the pressure distributions at five different radial locations along the blades when operating in 10 and 25m/s winds, respectively. The distribution of pressure coefficient computed using the KAIST RANS code is compared with the data obtained during the NREL experiment and with the predictions made by Sørensen [3]. The pressure coefficient presented in Figs. 5 and 6 is defined as

$$C_p = \frac{P_\infty - P_0}{\frac{1}{2}\rho(V_\infty^2 + (\Omega r)^2)}, \qquad (5)$$

where Ω is the angular velocity of the turbine. The predictions of the pressure coefficient over the surface of the blade at the three most outboard radial locations (0.63R, 0.8R and 0.95R) by the KAIST RANS code compare well with both the NREL experimental data and the RANS solution performed by Sørensen, as shown in Figs. 5(c), 5(d) and 5(e). At blade sections further inboard, there are substantial discrepancies between both the KAIST and Sørensen RANS solutions and the experimental data. It should be noted that the sharp gradients in pressure coefficient evident at the trailing edge of the blade in Figs. 5 and 6 in the KAIST RANS simulations result from the use of a hybrid mesh within the solution domain. The experimental data indicates that separation occurs at the leading edge at the 0.47R radial station. In contrast, both the KAIST and Sørensen Navier-Stokes solutions demonstrate poor correlation with the experimental data at this location and, in contrast, suggest the presence of a large suction peak at the leading edge, as shown in Fig. 5(b). The prediction of attached flow near the leading edge at the 0.47R radial station is confirmed by Fig. 7, in which the streamlines over the suction surface of the blade operating at wind speeds of 7, 10 and 25m/s are illustrated. In Fig. 7(b), the separation of the boundary layer from the suction surface manifests as the coalescence of streamlines between the quarter-chord and half-chord lines; indicating that the flow is predicted to be attached at chordwise locations closer to the leading edge.

At a wind speed of 25m/s, the flow over the suction surface of the blades is almost entirely separated, as indicated by the absence of a leading edge suction peak at any of the radial locations shown in Fig. 6. Indeed, the separation of the flow results in an almost uniform pressure distribution along the suction surface. Whilst the KAIST and Sørensen Navier-Stokes schemes predict the distribution of pressure coefficient similarly well over the majority of the blade, and agree well with the experimental data at the three most outboard radial locations, the KAIST RANS code underpredicts the pressure coefficient on the suction surface at the 0.47R radial station. Figure 7(c) shows that the flow over the suction surface of the blade at a wind speed of 25m/s is largely directed radially outboard toward the tip of the blade, and indicates that the flow aft of the separation line is strongly influenced by centrifugal effects. This finding is consistent with the findings of Sørenesen [3], and is in contrast to the almost entirely chordwise flow over the blades when operating in a 7m/s wind, as shown in Fig. 7(a). Importantly, the distributions of velocity and pressure

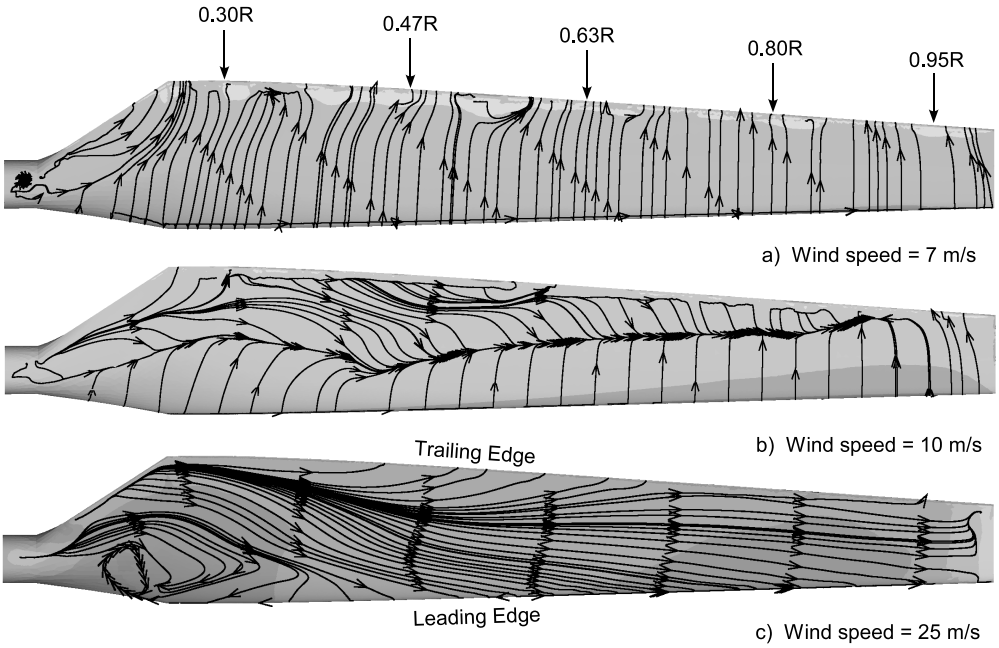

Figure 7: *Streamlines computed using the KAIST RANS solver on the surface of the blade at three different wind speeds.*

over the wind turbine blade that are computed using 'traditional' CFD codes that solve the Navier-Stokes equations in primitive-variable form thus reinforce the physical basis for augmentation of the two-dimensional aerofoil data using a stall delay model when using the simpler blade aerodynamic model that is implemented within the VTM.

Wake Structure

By solving the governing equations of fluid motion in vorticity conservation form, the VTM can realistically simulate the global dynamics of the wake that is developed by the wind turbine, even after the associated vorticity has convected a significant distance downstream of the rotor. In contrast, computational schemes based on the solution of the RANS equations suffer from considerable numerical dissipation and spatial smearing of the vortical structures within their predicted wake. This dissipation can only be alleviated by using a computational domain in which a high cell density is maintained to significant distances from the rotor, or by using a mesh that is generated using a vortex-following procedure. Figure 8 shows instantaneous snapshots of the wake that is predicted by the VTM and KAIST RANS methods to develop downwind of the wind turbine rotor when operating in a 7m/s wind. The wake is represented by rendering a surface within the flow on which the vorticity has a constant magnitude. Figure 8(a) shows the wake computed using the VTM. The vorticity induced by each of the two blades is illustrated by using different shades of grey (light and dark). Figure 8(b) shows the equivalent wake computed using the KAIST RANS code.

Figures 8(a) and 8(b) demonstrate how concentrated vortices form behind the tips of the blades. Figure 8 also illustrates that both the VTM and the KAIST RANS code predict the formation of a concentrated vortex downwind of the root of the blade. Figure 8(a) demonstrates the persistence of the inboard vortex sheet that is computed using the VTM. This sheet gradually deforms to align more substantially with the freestream flow as the wake age increases. It should be noted that in the VTM the blades are modelled as finite wings with a root cut-out. As a result, the formation of concentrated vortices at the blade roots does not entirely reflect the formation of the complex vortex system that is generated downwind of the rotor hub by real wind turbines. The conservation of vorticity by the VTM allows the tip vortices to be resolved beyond the point at which instabilities manifest, as is evident in Fig. 8(a) approximately three rotor diameters downwind of the rotor. Figure 8(b) demonstrates the rapid loss of coherence of the tip vortex that occurs as a result of the numerical dissipation of vorticity within almost all RANS codes.

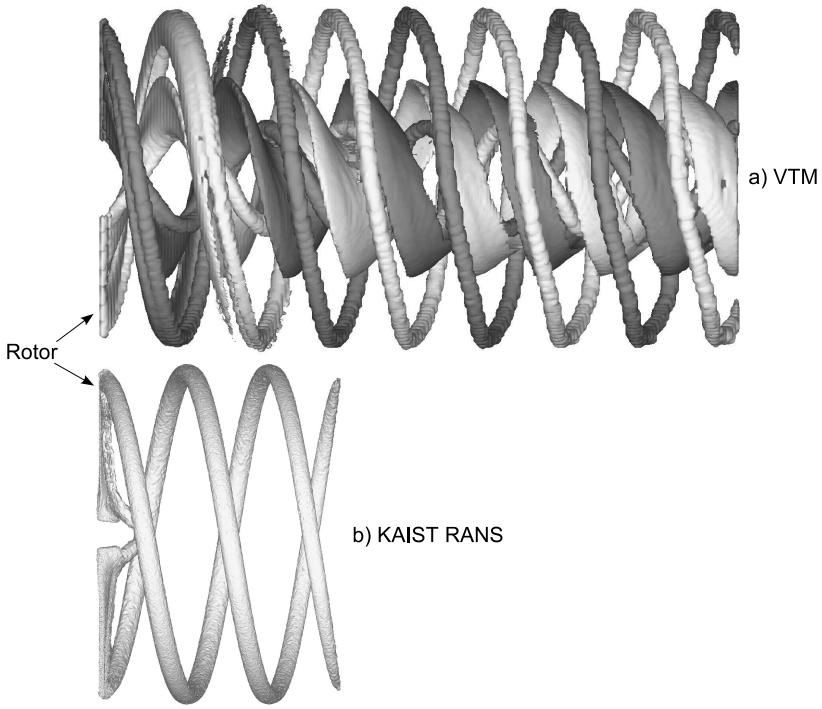

Figure 8: *Wake structure developed by the rotor when operating in a 7m/s wind (λ=5.4), rendered as a surface within the flow on which the vorticity has constant magnitude. The same vorticity magnitude has been used to render the wake structures predicted by both the VTM and the KAIST RANS code.*

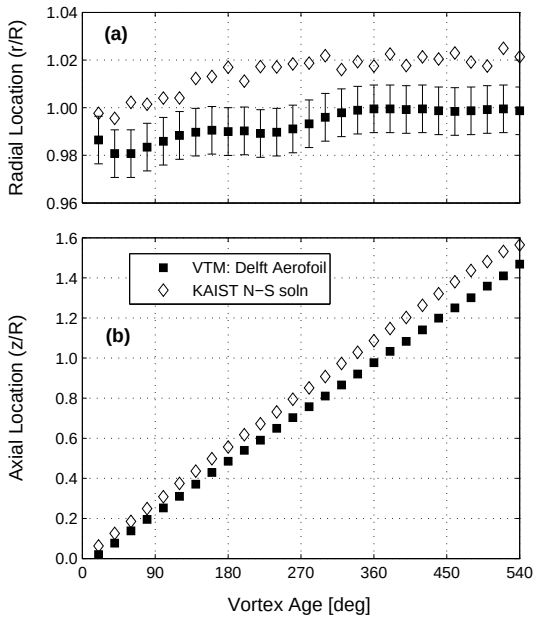

Figure 9: *Trajectory of tip vortices trailed by the rotor when operating in a 7m/s wind (λ=5.4).*

The evolution of the tip vortices is represented quantitatively in Fig. 9, in which the radial and axial coordinates of a representative tip vortex are plotted as a function of the vortex age. There is considerable uncertainty in the vortex positions determined using the VTM. This is a result of the relatively coarse grid on which the wake is evolved in the present simulations (50 cells per rotor radius), when compared to the grids on which the RANS equations are typically solved. The uncertainty is quantified in Fig. 9(a) by using bars that represent the cell edge-length, and therefore the possible error in the resolution of the position of the centre of the tip vortex. Figure 9(a) demonstrates that the wakes computed by both the VTM and KAIST RANS codes undergo a modest expansion in radius with increasing vortex age. The rates of radial expansion of the tip vortex predicted by the VTM and KAIST RANS codes are similar. A persistent offset in the radial location at which the tip vortex is predicted to form on the blade is shown in Fig. 9(a). This offset is likely to be caused by the differing representations of the roll-up of the tip vortices immediately behind the blade that are intrinsic to the VTM and RANS methods. Figure 9(b) demonstrates that there is

reasonable agreement between the axial rate of convection of the tip vortex that is computed by the VTM and RANS codes. The slightly higher rate of convection predicted by the RANS method compared to the VTM is consistent with its more rapid numerical dissipation, and hence the lessened effect of self-induced velocity in reducing the pitch of the helical tip vortex.

Conclusion

A Vorticity Transport Model and a computational scheme that solves the Reynolds-Averaged Navier-Stokes equations in pressure-velocity-density form have been validated against data from Phase VI of the NREL Unsteady Aerodynamics Experiment. The VTM can be run using a relatively coarse aerodynamic discretisation in order to obtain computationally efficient predictions of the performance of wind turbines. Simulations that were performed using the VTM, with a finer discretisation of the wake, have revealed the subtle characteristics of the vortex filaments, and the changes in wake structure that result from the natural instability of the vortices. Reynolds-Averaged Navier-Stokes schemes are able to provide, in general, accurate predictions of the aerodynamic loading on the blades, and the velocity and pressure fields surrounding the blades from first principles, but carry a relatively high computational burden. In the short term, computational aerodynamics tools such as the VTM and RANS schemes may be used to complement each other by providing designers with a greater knowledge of the aerodynamic behaviour of wind turbines than can be obtained by using either method in isolation. In the longer term, constant improvements in computing facilities may eventually allow the use of hybrid schemes that inherit at least some of the advantages offered by the VTM and RANS methods.

Acknowledgements

The authors would like to thank Pierre Widehem and Greg Bimbault of the Ecole Navale in France for the insights provided by their project work while visiting students at the Glasgow University.

References

[1]Hand, M.M., Simms, D.A., Fingersh, L.J., Jager, D.W., Cotrell, J.R., Schreck, S., Larwood, S.M. Unsteady Aerodynamics Experiment Phase VI: Wind Tunnel Test Configurations and Available Data Campaigns. NREL TP-500-29955 2001.

[2]Sezer-Uzol, N., Long, L. N. 3-D Time-Accurate CFD Simulations of Wind Turbine Rotor Flow Fields. AIAA Paper 2006-0394, AIAA Aerospace Sciences Meeting, Reno, NV, 2006.

[3]Sørensen, N.N., Michelsen, J.A., Schreck, S. Navier-Stokes Predictions of NREL Phase VI Rotor in the NASA Ames 80 ft x 120 ft Wind Tunnel. *Wind Energy* 2002, **5**, (2–3): 151–169.

[4]Brown, R.E. Rotor Wake Modeling for Flight Dynamic Simulation of Helicopters. *AIAA J.* 2000; **38**, (1): 57–63.

[5]Brown, R.E., Line, A.J. Efficient High-Resolution Wake Modeling using the Vorticity Transport Equation. *AIAA J.* 2005; **43**, (7): 1434–1443.

[6]Jung, M. S., Kown, O. J., Kang, H. J. Assessment of Rotor Hover Performance Using a Node-Based Flow Solver. *KSAS International Journal* 2007; **8**, (2): 44-53.

[7]Kang, H.J., Kwon, O.J. Unstructured Mesh Navier-Stokes Calculations of the Flow Field of a Helicopter Rotor in Hover. *J. of American Helicopter Soc.* 2002; **47**, (2): 90–99.

[8]Chorin, A.J. A Numerical Method for Solving Incompressible Viscous Flow Problems. *J. of Computational Physics* 1967; **2**, (12): 12–26.

[9]Butterfield, C. P., Scott, G., Musial, W. Comparison of Wind Tunnel Airfoil Performance Data with Wind Turbine Blade Data. Energy Conversion Engineering Conference, 1990.

[10]Duque, E.P.N, Burkland, M.D., Johnson, W. Navier-Stokes and Comprehensive Analysis Performance Predictions of the NREL Phase VI Experiment. *J. of Solar Energy Eng.* 2003; **125**, (4): 457–467.

[11]Breton, S., Coton, F.N., Moe, G. A Study on Rotational Effects and Different Stall Delay Models Using a Prescribed Wake Vortex Scheme and NREL Phase VI Experiment Data. *Wind Energy* 2008; **11**, (5): 459–482.

[12]Somers, D.M. Design and Experimental Results for the S809 Airfoil. 1989, Airfoils, Inc., State College, PA.

[13]Corrigan, J. J., Schillings, J. J. Empirical Model for Stall Delay due to Rotation. American Helicopter Society Aeromechanics Specialists Conference, San Francisco, CA, 1994.